

• 临床研究 •

临床特征联合 IVIM-DWI 参数对冻融胚胎移植患者早期妊娠结局的预测价值

邵文慧¹, 宋佳成¹, 张爱宁¹, 陆 遥¹, 徐义程², 陈 婷¹, 王 菁³, 马 翔³, 吴飞云^{1*}¹南京医科大学第一附属医院放射科, 江苏 南京 210029; ²西门子医疗磁共振研究合作中心, 上海 200082; ³南京医科大学第一附属医院生殖中心, 江苏 南京 210029

[摘要] 目的: 探讨临床特征联合体素内不相干运动弥散序列(intravoxel incoherent motion diffusion-weighted imaging, IVIM-DWI)参数在冻融胚胎移植(frozen-thawed embryo transfer, FET)患者早期妊娠结局中的预测价值。方法: 前瞻性纳入2023年12月—2025年1月在南京医科大学第一附属医院生殖中心行冻融胚胎移植的70例不孕女性患者, 均在胚胎移植日行标准化盆腔磁共振(magnetic resonance imaging, MRI)平扫检查。收集患者的临床及实验室指标、胚胎移植日的MRI常规特征及IVIM-DWI参数。使用FireVoxel软件提取IVIM-DWI的3个参数(水分子扩散系数D、灌注相关扩散系数D*、灌注分数f), 使用SPSS软件生成各个参数的直方图数据。采用t检验、Pearson卡方检验或Fisher精确检验比较临床妊娠组和未妊娠组患者的临床特征、常规MRI特征及IVIM-DWI参数的差异。使用受试者工作特征(receiver operating characteristic, ROC)曲线, 以曲线下面积(area under the curve, AUC)、DeLong检验评估各参数的诊断价值。使用多因素Logistic回归分析相关指标与受试者临床妊娠结局之间的关系。结果: 临床妊娠组42例, 未妊娠组28例。临床妊娠组优质胚胎的比例高于未妊娠组[76.2% vs. 46.4%, $P=0.011$]。临床妊娠组的子宫结合带D*_{mean}高于未妊娠组(45.233±7.930 vs. 41.223±6.369, $P=0.029$)。胚胎等级(优质胚胎)预测FET患者妊娠成功的AUC为0.65, 灵敏度和特异度分别为53.6%和73.2%; 子宫结合带D*_{mean}预测妊娠成功的AUC为0.68, 灵敏度73.8%, 特异度67.9%。胚胎等级联合子宫结合带D*_{mean}具有最优的预测效能, AUC为0.73, 灵敏度82.1%, 特异度60.0%。子宫结合带D*_{mean}值 $<43.33 \times 10^{-3} \text{ mm}^2/\text{s}$ (OR=0.2, $P=0.003$)是FET患者临床妊娠成功的独立危险因素。结论: IVIM-DWI可无创评估FET患者子宫微循环灌注状态, 子宫结合带D*_{mean}联合胚胎质量参数可提高FET患者临床妊娠结局的预测效能。

[关键词] 体外受精-胚胎移植; 磁共振成像; 体素内不相干弥散; 妊娠结局

[中图分类号] R445.2

[文献标志码] A

[文章编号] 1007-4368(2025)10-1476-11

doi: 10.7655/NYDXBNSN250516

The predictive value of clinical features combined with IVIM-DWI parameters for early pregnancy outcomes in frozen-thawed embryo transfer patients

SHAO Wenhui¹, SONG Jiacheng¹, ZHANG Aining¹, LU Yao¹, XU Yicheng², CHEN Ting¹, WANG Jing³, MA Xiang³, WU Feiyun^{1*}¹Department of Radiology, the First Affiliated Hospital of Nanjing Medical University, Nanjing 210029; ²MR Research Collaboration, Siemens Healthineers, Shanghai 200082; ³Reproductive Medicine Center, the First Affiliated Hospital of Nanjing Medical University, Nanjing 210029, China

[Abstract] **Objective:** To investigate the predictive value of clinical features combined with intravoxel incoherent motion diffusion-weighted imaging(IVIM-DWI)parameters for early pregnancy outcomes in patients undergoing frozen-thawed embryo transfer(FET). **Methods:** This prospective study enrolled 70 infertile women who underwent FET at the Reproductive Center of the First Affiliated Hospital of Nanjing Medical University between December 2023 and January 2025. All participants underwent standardized pelvic magnetic resonance imaging(MRI)scans on the day of embryo transfer. Clinical and laboratory indicators, as well as conventional MRI features and IVIM-DWI parameters were collected. IVIM-DWI parameters (diffusion coefficient D, pseudodiffusion coefficient D*, and

[基金项目] 江苏省科教能力提升工程(JSDW202243)

*通信作者(Corresponding author), E-mail: wfy_njmu@163.com(ORCID: 0000-0002-0343-0458)

perfusion fraction f) were extracted using FireVoxel software, with histogram data generated via SPSS. Student's t -test, Pearson's chi-square test, or Fisher's exact test were employed to compare differences in clinical characteristics, MRI features, and IVIM-DWI parameters between the clinical pregnancy group and the non-pregnant group. Receiver operating characteristic (ROC) curves were constructed to quantify diagnostic performance using area under the curve (AUC) measurements, with statistical comparisons performed by DeLong's test. Multivariate logistic regression was used to analyze the relationship between relevant indicators and clinical pregnancy outcomes. **Results:** The clinical pregnancy group comprised 42 cases, while the non-pregnant group had 28 cases. The proportion of high-quality embryos in the clinical pregnancy group was higher than that in the non-pregnant group [76.2% vs. 46.4%, $P=0.011$]. The junctional zone D_{mean}^* was significantly higher in the clinical pregnancy group than that in the non-pregnant group (45.233 ± 7.930 vs. 41.223 ± 6.369 , $P=0.029$). ROC analysis revealed that embryo quality (high-grade embryos) predicted pregnancy success with an AUC of 0.65 (sensitivity 53.6%, specificity 73.2%), while junctional zone D_{mean}^* achieved an AUC of 0.68 (sensitivity 73.8%, specificity 67.9%). The combination of embryo quality and junctional zone D_{mean}^* demonstrated superior predictive efficacy (AUC=0.73, sensitivity 82.1%, specificity 60.0%). Junction zone $D_{\text{mean}}^* < 43.33 \times 10^{-3} \text{ mm}^2/\text{s}$ was identified as an independent risk factor for successful clinical pregnancy (OR=0.2, $P=0.003$). **Conclusion:** IVIM-DWI enables noninvasive assessment of microcirculatory perfusion characteristics of FET patients. Combining embryo quality with junctional zone D_{mean}^* enhances the prediction of clinical pregnancy outcomes.

[Key words] *in vitro* fertilization-embryo transfer; magnetic resonance imaging; intravoxel incoherent motion; pregnancy outcome

[J Nanjing Med Univ, 2025, 45(10): 1476-1486]

2023年我国不孕不育患者约占成年人口的1/6, 并呈逐年上升趋势^[1]。体外受精-胚胎移植(*in vitro* fertilization-embryo transfer, IVF-ET)是目前治疗不孕不育的主要手段,但移植成功率仅45%~57%^[2]。而冻融胚胎移植(frozen embryo transfer, FET)作为IVF-ET的重要补充技术,尽管可规避卵巢过度刺激风险,但其成功率仍受限于胚胎质量与子宫内膜容受性(endometrial receptivity, ER)的协同作用^[3]。ER是指子宫内膜允许胚胎定位、黏附、侵入,并使之着床的能力。ER的核心在于子宫内膜微循环灌注状态及血流动力学特征,尤其是在种植窗(window of implantation, WOI)期间,子宫内膜的血管重塑能力直接影响胚胎着床效率^[4]。因此,精准评估ER并预测FET妊娠结局,对优化移植时机、提升妊娠率具有重要临床意义。

超声因其无创性、安全性、实时性等优势,被认为是评估ER的首选方法^[5-6]。前期研究主要基于多普勒超声对子宫动脉、脐动脉等大血管的评估。Sliva等^[7]发现,在整个妊娠过程中,成功妊娠妇女的子宫动脉阻力指数(resistance index, RI)、搏动指数(pulsatility index, PI)均低于妊娠失败妇女。Wang等^[8]分析显示,在人绒毛膜促性腺激素(human chorionic gonadotropin, HCG)注射日,妊娠妇女子宫内各项血流参数包括血管化指数(vascularization index, VI)、血流指数(flow index, FI)和血管化血

流指数(vascularization flow index, VFI)均显著高于未妊娠组。但是作为胚胎着床接触部位,内膜及内膜下微血流灌注也是影响妊娠结局的最直接因素^[9]。然而超声直接评估内膜微循环血流灌注的能力有限,有研究者用超声微泡造影对子宫内膜微循环血流灌注进行评估,不孕症患者子宫内膜及内膜下微血管密度(microvessel density, MVD)显著低于健康女性^[10]。但是超声微泡造影是有创检查,且需要注射造影剂,不适合在临近移植日进行检查,超声检查对操作者经验依赖性也较高。因此,临床上急需无创、安全可靠、高效准确评估ER的检查手段。

磁共振(magnetic resonance imaging, MRI)成像因其多方位、多序列、多参数成像的特点对子宫内膜形态学及功能学改变具有特殊的成像优势。随着MRI功能序列的发展,如弥散加权成像(diffusion weighted imaging, DWI)、体素内不相关运动弥散成像(intravoxel incoherent motion diffusion-weighted imaging, IVIM-DWI)等成像技术从微观层面观察子宫内膜微结构以及微循环血流灌注等信息,成为评估子宫内膜病变微观改变的重要检查手段。IVIM-DWI通过分离水分子扩散与微循环灌注,可无创量化子宫内膜血流动力学特征:水分子扩散系数(D)可以反映细胞外间隙中水分子的真实扩散;灌注相关扩散系数(D*)主要反映微循环血流灌注容量,被认为与毛细血管的密度及血流速度有关;灌注分数

(f)主要代表感兴趣区局部微循环所致的灌注,与血管的生成及微血管的通透性有关。IVIM-DWI序列目前已广泛应用于评估胎盘、肿瘤、卒中等微循环灌注^[11-14]。在月经周期不同阶段子宫内膜IVIM参数具有差异性^[15]。内膜在WOI期间经历显著的血管重塑与血流动力学变化,其微循环改变很可能是影响妊娠结局的一个重要因素。

因此,本研究旨在通过对比早期临床妊娠组与未妊娠组移植当日的IVIM-DWI参数(D、D*、f)差异,结合常规MRI形态学特征及胚胎质量分级,探索临床特征、常规MRI特征联合IVIM-DWI的微循环血流灌注参数对FET妊娠结局的预测价值,为临床优化FET移植时机提供无创、精准的影像学依据。

1 对象和方法

1.1 对象

本研究是前瞻性研究,经医院伦理委员会批准通过(伦理批号:2025-SRFA-416),所有患者均签署知情同意书。纳入了2023年12月—2025年1月南京医科大学第一附属医院生殖中心行FET的不孕女性患者77例,均在胚胎移植日清晨行标准化盆腔MRI平扫检查。纳入标准:①年龄20~45岁;②体外受精胚胎移植中第1~2次冻胚移植;③临床资料及实验室检查完整,患者和家属可配合整个治疗、检查、随访等。排除标准:①幽闭恐惧症;②MRI禁忌(如体内有心脏起搏器和金属植入物);③患有宫腔发育畸形、中重度子宫内膜异位症、子宫多发肌瘤、宫腔粘连等严重影响胚胎种植疾病;④合并传染病或有严重的内外科疾病等;⑤失访、无移植结局;⑥MRI图像差。最终共纳入70例患者。

收集患者的临床及实验室数据、常规MRI特征、IVIM-DWI参数。临床及实验室数据包括:年龄、体重指数(body mass index, BMI)、不孕时间、不孕类型、内膜准备情况、生育史、移植胚胎类型及质量、移植当天雌二醇(estradiol, E2)水平及孕酮(progesterone, P)水平。常规MRI特征包括T2WI图像测量子宫内膜、结合带和肌层的厚度、最大层面内膜面积;T2WI子宫内膜相对信号强度;子宫位置(前位/后位)。IVIM-DWI参数(D、D*、f),常规DWI参数的表现弥散系数(apparent diffusion coefficient, ADC)。

1.2 方法

1.2.1 MRI数据采集

使用3.0T磁共振扫描仪(Magnetom Skyra, 西门子公司, 德国)进行检查。采用18通道相控阵腹部

线圈。所有患者均在移植当日清晨行标准化盆腔MTI检查。为了减少肠道蠕动,要求患者在MRI扫描前需禁食至少4 h。扫描序列包括:矢状位T2WI图像:重复时间/回波时间2 700 ms/106 ms,分辨率0.8 mm×0.8 mm×4.0 mm,视野240 mm×240 mm;轴位T2WI图像:重复时间/回波时间2 550 ms/87 ms,分辨率1.0 mm×0.8 mm×4.0 mm,视野240 mm×240 mm;轴向T1WI图像:重复时间/回波时间500 ms/9.9 ms,分辨率1.0 mm×0.7 mm×4.0 mm,视野240 mm×240 mm;轴位IVIM(b值:0、50、100、150、200、500、1 000 s/mm²)图像:重复时间/回波时间6 800 ms/98 ms,分辨率1.8 mm×1.5 mm×5.0 mm,视野240 mm×240 mm。

1.2.2 常规MRI特征的提取

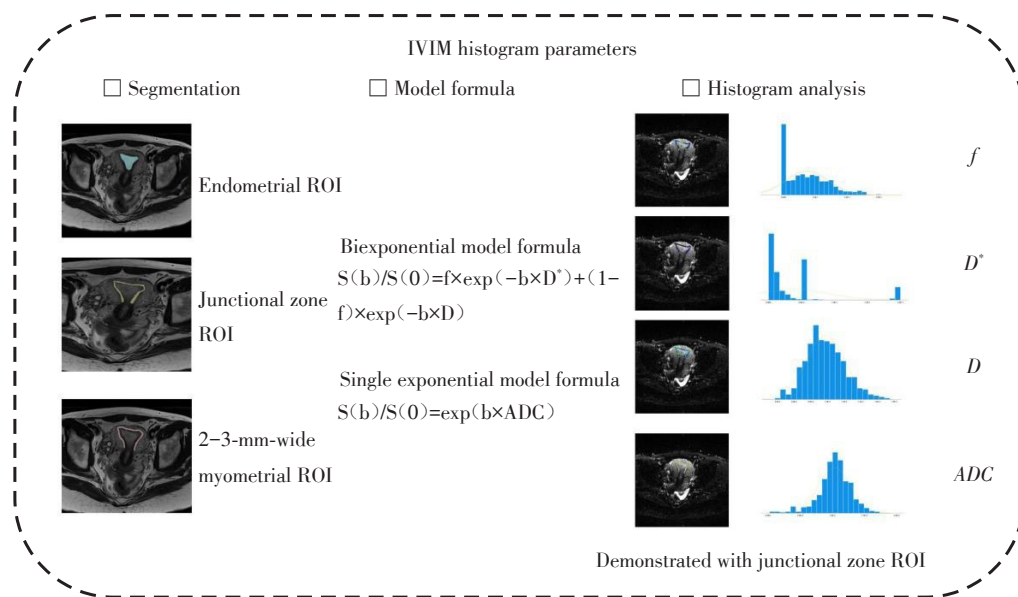
根据矢状位T2WI图像在子宫最大截面图像上测量子宫内膜、结合带、肌层厚度:子宫内膜厚度取内膜前后壁最远距离;子宫结合带厚度取结合带最宽处,子宫肌层厚度取子宫前后壁肌层与结合带连接处最厚处的距离,并测量子宫颈体交界处距宫颈管口的距离及子宫内膜的最大面积。以上数据由具有盆腔MRI诊断经验3年和10年的2位放射科医生独立测量3次取平均值。在矢状位T2WI图像上判断子宫位置(前位子宫/后位子宫)。在轴位图像上计算最大截面子宫内膜与竖脊肌的T2WI的相对强度信号。

1.2.3 IVIM-DWI参数的提取

根据轴位IVIM-DWI图像在子宫最大截面确定感兴趣区域(region of interest, ROI),根据解剖结构调整测量范围,在子宫肌层上精细地绘制2~3 mm宽的ROI及该层面子宫内膜和结合带ROI。将图像导入FireVoxel软件(纽约大学,美国)对多b值扩散加权图像进行IVIM-DWI的后处理。采用双指数模型公式 $S(b)/S(0)=f \times \exp(-b \times D^*)+(1-f) \times \exp(-b \times D)$ (方程1),计算f、D和D*。使用所有b值对方程1进行体素拟合,生成f、D和D*的参数图。DWI模型的 $S(b)/S(0)=\exp(b \times \text{ADC})$ (方程2),ADC值由b=0和1 000 s/mm²计算生成。然后使用SPSS27.0软件对参数进行直方图分析,计算各参数的平均值、第10百分位数及第90百分位数。IVIM直方图分析流程图见图1。

1.2.4 胚胎质量等级评估

由1名有10年工作经验的生殖科医生进行胚胎质量等级的评估。卵裂期胚胎评估:胚胎发育速度正常,卵裂球对称,数目均等或大致均等,细胞质均匀,碎片占比<10%,定义为优质胚胎。囊胚期胚胎



This figure shows the three research links of IVIM histogram parameters. ROI drawing: Based on the axial IVIM-DWI image, the ROI images of the endometrium, the junction zone and the 2-3 mm wide myometrium are determined in the largest cross-section of the uterus. Model construction: The images are post-processed on the FireVoxel software using the biexponential model: $S(b)/S(0)=f \times \exp(-b \times D^*) + (1-f) \times \exp(-b \times D)$ and the single exponential model: $S(b)/S(0)=\exp(b \times ADC)$. Histogram analysis: SPSS software is used to perform histogram analysis on the parameters. The above figure takes the junction zone ROI as an example to show the histogram distribution of f , D^* , D and ADC parameters, which are used to quantitatively analyze the tissue microstructure and blood perfusion characteristics.

图1 IVIM直方图分析流程图

Figure 1 Flowchart of IVIM histogram analysis

评估: 根据 Gardner 评分标准, 依据囊胚扩张程度, 将囊胚分成 1~6 级; 依据内细胞团质量, 评分 A、B、C 级; 依据滋养层细胞质量, 评分 A、B、C 级。将 D5 评分 $\geq 3BB$ 或者 D6 评分 $\geq 4BB$ 的囊胚定义为优质囊胚^[16]。

1.2.5 妊娠结局判定

临床妊娠: 移植 2 周后血 β -HCG 水平显著上升, 且于移植 4 周后阴道超声检查可见妊娠囊。临床未妊娠: 移植后第 14 天抽血检测 β -HCG 水平, 若 HCG 阴性, 移植后 4 周阴道超声检查未见妊娠囊则判定未妊娠。

1.3 统计学方法

采用 SPSS37.0 统计软件进行数据分析。采用 Kolmogorov-Smirnov 检验评价参数是否服从正态分布。满足正态分布的连续性变量采用独立样本 t 检验, 以均数 \pm 标准差 ($\bar{x} \pm s$) 表示; 不满足正态分布的连续性变量采用 Mann-Whitney U 检验, 以中位数 (四分位数) [$M(P_{25}, P_{75})$] 表示。分类变量采用卡方检验, 以 [$n(\%)$] 表示。采用受试者工作特征 (receiver operating characteristic, ROC) 曲线, 以曲线下面积 (area under the curve, AUC)、DeLong 检验评估各参数的诊断价值, 并计算连续变量的最佳 cut-off 值。采用多因素 Logistic 回归分析相关指标与受试

者临床妊娠结局之间的关系。 $P < 0.05$ 为差异有统计学意义。

2 结果

2.1 两组患者临床特征的比较

本研究最终纳入了行 FET 的不孕症女性患者 70 例, 其中临床妊娠组 42 例, 未妊娠组 28 例。患者的基线临床特征如表 1 所示, 临床妊娠组优质胚胎的比例高于未妊娠组 [76.2% vs. 46.4%, $P=0.011$]。临床妊娠组移植胚胎类型 (卵裂期/囊胚期) 与未妊娠组的差异具有统计学意义 [33.3% vs. 10.7%, $P=0.031$]。两组患者的年龄、BMI、不孕时间、不孕原因、男方因素、内膜准备、既往生育史、E2、P 差异均无统计学意义 ($P > 0.05$)。

2.2 两组间常规 MRI 特征的比较

子宫内膜厚度、结合带厚度、肌层厚度、宫颈长度、子宫内膜最大层面的面积、子宫内膜 T2WI 相对信号强度、子宫位置 (前位/后位) 在两组患者间差异均无统计学意义 ($P > 0.05$, 表 2)。

2.3 两组间 IVIM-DWI 参数的比较

早期临床妊娠组的子宫结合带 D^*_{mean} 高于未妊娠组 (45.233 ± 7.930 vs. 41.223 ± 6.369 , $P=0.029$); 早

期临床妊娠组的子宫结合带 D_{90th}^* 高于未妊娠组 ($P=0.032$)。子宫内膜、肌层的IVIM直方图参数及子宫结合带 D_{mean} 、 D_{10th} 、 D_{90th} 、 f_{mean} 、 f_{90th} 在两组间均无统计学差异 ($P > 0.05$, 表3, 图2)。图3是胚胎质量均为优质胚胎的2例入组患者, 早期临床妊娠组的子宫结合带的 D_{mean}^* 和 D_{90th}^* 高于未妊娠组, 提示子宫结合带的 D_{mean}^* 和 D_{90th}^* 值有望成为FET患者早期临床妊娠

成功的潜在生物学指标。

2.4 两组间ADC参数的比较

子宫内膜、结合带及肌层的ADC直方图参数在两组患者间差异均无统计学意义 ($P > 0.05$, 表3)。

2.5 临床特征及IVIM-DWI参数预测FET患者早期妊娠成功的效能评估

胚胎等级(优质胚胎)预测FET患者妊娠成功

表1 临床妊娠组及未妊娠组临床特征比较

Table 1 Comparison of clinical characteristics between the clinical pregnancy group and non-pregnant group

Variable	Clinical pregnancy group (n=42)	Non-pregnant group (n=28)	P
Age[years, ($\bar{x} \pm s$)]	32.86 \pm 3.89	32.79 \pm 4.29	0.943
BMI[kg/m ² , $M(P_{25}, P_{75})$]	22.15(19.25, 25.33)	22.50(20.75, 24.82)	0.569
Infertility duration[years, $M(P_{25}, P_{75})$]	3.3(2.3, 4.5)	3.3(2.4, 4.3)	0.952
Infertility causes[n(%)]			0.198
Primary	22(52.3)	19(67.9)	
Secondary	20(47.6)	9(32.1)	
Male factor[n(%)]			1.000
Present	5(11.9)	3(10.7)	
Absent	37(88.1)	25(89.3)	
Endometrial preparation[n(%)]			0.270
Natural Cycle	14(33.3)	13(46.4)	
Artificial Cycle	28(66.7)	15(53.6)	
Previous heproductive history[n(%)]			0.947
Present	6(14.3)	5(17.9)	
Absent	36(85.7)	23(82.1)	
E2[pmol/L, $M(P_{25}, P_{75})$]	440.90(296.75, 740.13)	671.05(349.33, 927.35)	0.270
P[nmol/L, $M(P_{25}, P_{75})$]	39.01(25.95, 52.00)	43.34(27.56, 66.91)	0.401
Embryo transfer stage[n(%)]			0.031
Cleavage stage	14(33.3)	3(10.7)	
Blastocyst stage	28(66.7)	25(89.3)	
Embryo quality[n(%)]			0.011
High-quality	32(76.2)	13(46.4)	
Suboptimal	10(23.8)	15(53.6)	

表2 临床妊娠组及未妊娠组MRI常规特征比较

Table 2 Comparison of MRI routine features between the clinical pregnancy group and non-pregnant group

Variable	Clinical pregnancy group (n=42)	Non-pregnant group (n=28)	P
Endometrial thickness[mm, $M(P_{25}, P_{75})$]	8.2(6.5, 11.5)	7.6(5.5, 9.4)	0.17
Junctional zone thickness[mm, $M(P_{25}, P_{75})$]	7.6(5.5, 9.4)	5.1(4.3, 6.0)	0.22
Myometrial thickness(mm, $\bar{x} \pm s$)	11.38 \pm 2.73	11.43 \pm 2.37	0.94
Cervical length[mm, $M(P_{25}, P_{75})$]	27.00(25.50, 30.40)	30.15(25.80, 32.75)	0.12
Maximum endometrial area[mm ² , $M(P_{25}, P_{75})$]	325.00(235.50, 415.60)	286.60(183.05, 362.55)	0.23
Endometrial T2WI signal ratio($\bar{x} \pm s$)	4.34 \pm 0.90	4.47 \pm 0.93	0.55
Uterine position[n(%)]			0.77
Anteverted	21(50.0)	15(53.6)	
Retroverted	21(50.0)	13(46.4)	

的ROC曲线下面积为0.65,灵敏度和特异度分别为53.6%和73.2%;子宫结合带 D_{mean}^* 预测临床妊娠成功的AUC为0.68,灵敏度73.8%,特异度67.9%,优于结合带 $D_{90\text{th}}^*$ 的预测效能(AUC=0.65)。胚胎等级联合结合带 D_{mean}^* 具有最优的预测效能, AUC为0.73,灵敏度82.1%,特异度60.0%(表4,图4)。DeLong检验提示,胚胎等级联合子宫结合带 D_{mean}^* 预测模型与胚胎等级预测模型比较,差异具有统计学意义($Z=2.041, P < 0.05$)。胚胎等级联合子宫结合

带 D_{mean}^* 预测模型与子宫结合带 D_{mean}^* 预测模型相比,差异无统计学意义($Z=1.024, P > 0.05$)。

2.6 FET患者临床妊娠成功的多因素Logistic回归分析

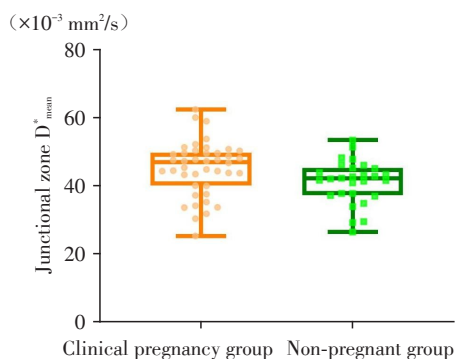
根据子宫结合带 D_{mean}^* cut-off值 $43.33 \times 10^{-3} \text{ mm}^2/\text{s}$,将受试者分为高子宫结合带 D_{mean}^* 组($D_{\text{mean}}^* \geq 43.33 \times 10^{-3} \text{ mm}^2/\text{s}$)及低子宫结合带 D_{mean}^* 组($D_{\text{mean}}^* < 43.33 \times 10^{-3} \text{ mm}^2/\text{s}$)。多因素Logistic回归结果显示,子宫结合带 D_{mean}^* 值 $< 43.33 \times 10^{-3} \text{ mm}^2/\text{s}$ 是FET患者临床妊

表3 临床妊娠组及未妊娠组IVIM直方图参数比较

Table 3 Comparison of IVIM histogram parameters between the clinical pregnancy group and non-pregnant group

Variable	Clinical pregnancy group (n=42)	Non-pregnant group (n=28)	P
Endometrium			
$D_{\text{mean}}^* [\times 10^{-3} \text{ mm}^2/\text{s}, M(P_{25}, P_{75})]$	35.022(32.255, 45.462)	44.451(38.840, 47.534)	0.134
$D_{90\text{th}}^* [\times 10^{-3} \text{ mm}^2/\text{s}, M(P_{25}, P_{75})]$	54.493(54.453, 186.376)	185.706(54.482, 195.934)	0.239
$D_{\text{mean}} [\times 10^{-3} \text{ mm}^2/\text{s}, M(P_{25}, P_{75})]$	1.178(1.102, 1.346)	1.156(1.080, 1.291)	0.557
$D_{10\text{th}} [\times 10^{-3} \text{ mm}^2/\text{s}, M(P_{25}, P_{75})]$	0.803(0.627, 0.969)	0.899(0.711, 0.948)	0.502
$D_{90\text{th}} [\times 10^{-3} \text{ mm}^2/\text{s}, M(P_{25}, P_{75})]$	1.515(1.370, 1.724)	1.459(1.376, 1.610)	0.338
$f_{\text{mean}} [\%, M(P_{25}, P_{75})]$	13.961(10.669, 19.467)	12.787(11.122, 15.751)	0.701
$f_{90\text{th}} [\%, M(P_{25}, P_{75})]$	29.875(25.335, 38.823)	29.520(26.220, 37.098)	0.783
$ADC_{\text{mean}} [M(P_{25}, P_{75})]$	1.396(1.272, 1.633)	1.356(1.280, 1.497)	0.308
$ADC_{10\text{th}} (\bar{x} \pm s)$	1.085 \pm 0.203	1.033 \pm 0.163	0.270
$ADC_{90\text{th}} [M(P_{25}, P_{75})]$	1.758(1.572, 1.996)	1.727(1.573, 1.864)	0.381
Junction zone	45.233 \pm 7.930	41.223 \pm 6.369	0.029
$D_{\text{mean}}^* [\times 10^{-3} \text{ mm}^2/\text{s}, (\bar{x} \pm s)]$			
$D_{90\text{th}}^* [\times 10^{-3} \text{ mm}^2/\text{s}, M(P_{25}, P_{75})]$	174.605(54.476, 192.058)	54.476(54.429, 185.706)	0.032
$D_{\text{mean}} [\times 10^{-3} \text{ mm}^2/\text{s}, (\bar{x} \pm s)]$	0.733 \pm 0.155	0.789 \pm 0.203	0.198
$D_{10\text{th}} [\times 10^{-3} \text{ mm}^2/\text{s}, M(P_{25}, P_{75})]$	0.229(0.140, 0.431)	0.344(0.140, 0.538)	0.208
$D_{90\text{th}} [\times 10^{-3} \text{ mm}^2/\text{s}, M(P_{25}, P_{75})]$	1.110(1.019, 1.234)	1.234(1.024, 1.310)	0.291
$f_{\text{mean}} [\%, (\bar{x} \pm s)]$	17.294 \pm 5.251	17.032 \pm 6.548	0.854
$f_{90\text{th}} [\%, M(P_{25}, P_{75})]$	45.582(37.146, 48.707)	42.089(35.917, 47.194)	0.443
$ADC_{\text{mean}} [M(P_{25}, P_{75})]$	0.939(0.873, 1.057)	1.021(0.893, 1.185)	0.128
$ADC_{10\text{th}} [M(P_{25}, P_{75})]$	0.416(0.327, 0.602)	0.496(0.373, 0.731)	0.128
$ADC_{90\text{th}} (\bar{x} \pm s)$	1.442 \pm 0.139	1.495 \pm 0.162	0.153
Myometrium	37.685(33.675, 46.887)	41.084(33.986, 46.887)	0.783
$D_{\text{mean}}^* [\times 10^{-3} \text{ mm}^2/\text{s}, M(P_{25}, P_{75})]$			
$D_{90\text{th}}^* [\times 10^{-3} \text{ mm}^2/\text{s}, M(P_{25}, P_{75})]$	149.684(56.631, 196.074)	192.172(54.494, 196.050)	0.971
$D_{\text{mean}} [\times 10^{-3} \text{ mm}^2/\text{s}, (\bar{x} \pm s)]$	1.031 \pm 0.180	1.058 \pm 0.229	0.588
$D_{10\text{th}} [\times 10^{-3} \text{ mm}^2/\text{s}, (\bar{x} \pm s)]$	0.570 \pm 0.229	0.622 \pm 0.286	0.396
$D_{90\text{th}} [\times 10^{-3} \text{ mm}^2/\text{s}, (\bar{x} \pm s)]$	1.450 \pm 0.188	1.474 \pm 0.199	0.620
$f_{\text{mean}} [\%, (\bar{x} \pm s)]$	28.902 \pm 5.735	28.352 \pm 6.277	0.706
$f_{90\text{th}} [\%, M(P_{25}, P_{75})]$	55.979(47.940, 59.178)	55.020(45.406, 60.153)	0.684
$ADC_{\text{mean}} (\bar{x} \pm s)$	1.561 \pm 0.149	1.577 \pm 0.180	0.685
$ADC_{10\text{th}} (\bar{x} \pm s)$	1.122 \pm 0.204	1.119 \pm 0.261	0.962
$ADC_{90\text{th}} (\bar{x} \pm s)$	1.999 \pm 0.156	2.013 \pm 0.150	0.714

ADC_{10th}: 10th percentile of ADC; ADC_{90th}: 90th percentile of ADC; ADC_{mean}: mean ADC; D_{10th}: 10th percentile of D; D_{90th}: 90th percentile of D; D_{mean}: mean D; D_{mean}^{*}: mean D^{*}; D_{90th}^{*}: 90th percentile of D^{*}; f_{mean}: mean f; f_{90th}: 90th percentile of f.



The D^*_{mean} value of the junction zone in the clinical pregnancy group was higher than that in the non-pregnant group ($P=0.029$).

图2 早期临床妊娠组与未妊娠组子宫结合带 D^*_{mean} 比较的箱式图

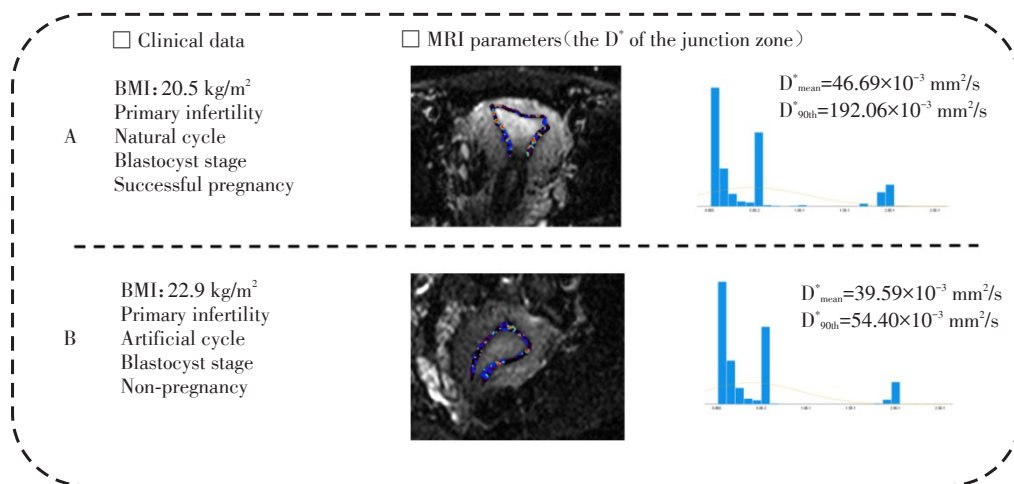
Figure 2 Box plot comparing junctional zone D^*_{mean} between the early clinical pregnancy group and non-pregnant group

娠成功的独立危险因素 ($OR=0.20, P=0.003$, 表5)。

基于结合带 D^*_{mean} 分层与胚胎质量(优质胚胎/次优胚胎)构建4组分析队列可以得出,高子宫结合带 D^*_{mean} ($D^*_{mean} \geq 43.33 \times 10^{-3} \text{ mm}^2/\text{s}$)联合优质胚胎组临床妊娠率最高(临床妊娠 vs. 未妊娠: 73% vs. 27%),组间差异接近统计学显著性 ($P=0.07$);低子宫结合带 D^*_{mean} ($D^*_{mean} < 43.33 \times 10^{-3} \text{ mm}^2/\text{s}$)联合次优胚胎组临床妊娠率最低(临床妊娠 vs. 未妊娠: 17% vs. 83%),组间差异有统计学意义 ($P < 0.001$, 图5)。

3 讨论

FET 技术为不孕不育患者提供了更多次移植、妊娠机会,超过 50%的早期妊娠因着床失败而导致流产,影响胚胎早期着床的因素较为复杂,包括临床激素水平、胚胎质量、内膜容受性等,子宫内膜容受性的准确评估,是辅助生殖技术的难点与重点。超声是目前临床应用最广泛的评估方法,但其对技



A: showed a woman diagnosed with primary infertility who achieved early clinical pregnancy with high-quality embryo. MRI parameters of the junctional zone: mean D^* : $46.69 \times 10^{-3} \text{ mm}^2/\text{s}$ (critical value: $43.33 \times 10^{-3} \text{ mm}^2/\text{s}$); 90th percentile of D^* : $192.06 \times 10^{-3} \text{ mm}^2/\text{s}$ (critical value: $54.48 \times 10^{-3} \text{ mm}^2/\text{s}$). Both parameters exceeded the critical values. B: showed a woman diagnosed with primary infertility who had an early clinical pregnancy failure and the embryo quality was high quality. MRI parameters of the junctional zone: mean D^* : $39.59 \times 10^{-3} \text{ mm}^2/\text{s}$ (critical value: $43.33 \times 10^{-3} \text{ mm}^2/\text{s}$); 90th percentile of D^* : $54.40 \times 10^{-3} \text{ mm}^2/\text{s}$ (critical value: $54.48 \times 10^{-3} \text{ mm}^2/\text{s}$). Both parameters were below the critical values.

图3 子宫结合带 D^*_{mean} 及 D^*_{90th} 在 2 例优质胚胎 FET 患者不同妊娠结局中的预测价值

Figure 3 Predictive value of D^*_{mean} and D^*_{90th} in different pregnancy outcomes of two FET patients with high quality embryo

表4 胚胎质量、子宫结合带 D^* 直方图参数预测早期临床妊娠结局的效能比较

Table 4 Comparison of embryo quality and the junctional zone D^* histogram parameters in predicting early clinical pregnancy outcomes

Variable	AUC(95%CI)	Cut-off value	Sensitivity(%)	Specificity(%)
Embryo quality	0.65(0.51-0.78)		53.6	73.2
Junction zone D^*_{mean}	0.68(0.55-0.81)	43.33×10^{-3}	73.8	67.9
Junction zone D^*_{90th}	0.65(0.52-0.79)	54.48×10^{-3}	61.9	67.9
Combined model	0.73(0.61-0.85)		82.1	60.0

Combined model: integrated model combining embryo quality and junctional zone mean D^* .

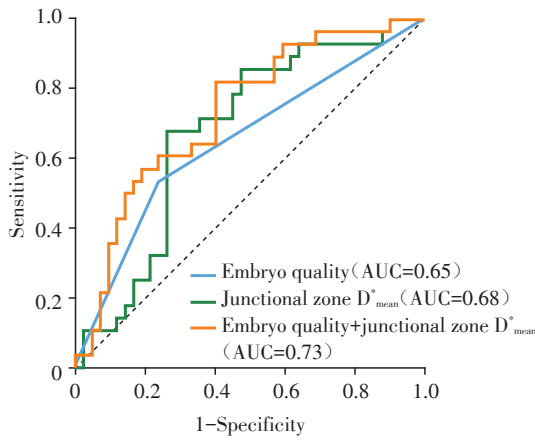


图4 胚胎质量、子宫结合带 D^*_{mean} 均值及两者联合模型预测早期临床妊娠结局的ROC曲线

Figure 4 ROC curves of embryo quality, junctional zone D^*_{mean} , and their combined models for predicting clinical pregnancy outcome

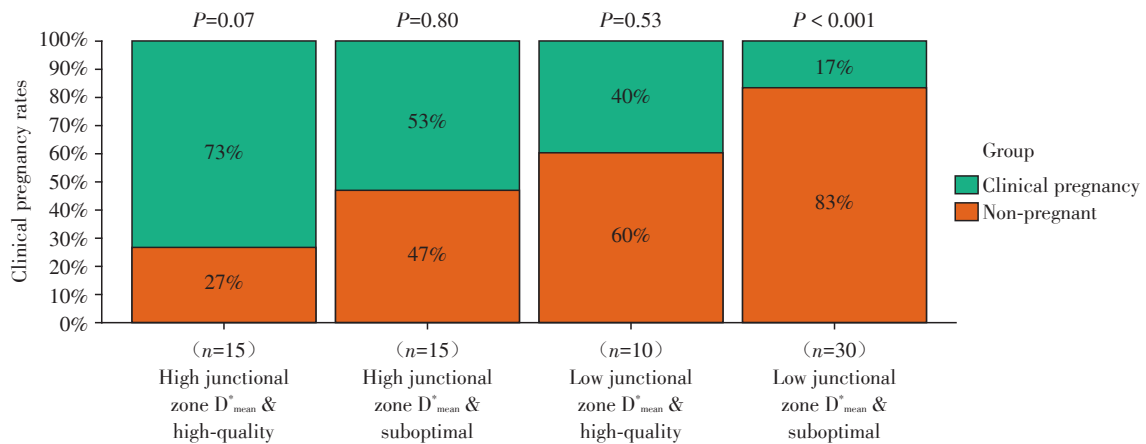


图5 子宫结合带 D^*_{mean} 与胚胎质量(优质/次优)的临床妊娠成功率比较

Figure 5 Comparison of clinical pregnancy rates stratified by junctional zone D^*_{mean} and embryo quality groups

了独特视角。本研究发现胚胎质量联合子宫结合带 D^*_{mean} 能提高FET患者临床妊娠结局的预测效能。

临床妊娠的成功取决于胚胎着床,近1/3的胚胎着床失败归因于胚胎质量^[3]。部分研究者认为囊胚期胚胎相对卵裂期胚胎具有更高的妊娠优势:①受精卵在输卵管段游走,在形成16细胞阶段的桑椹胚后到达子宫,至少相当于培育的第4天,因此第5天的囊胚期与自然妊娠周期更相近,子宫内膜与输卵管的环境相同,更有利于着床;②部分卵裂期胚胎存在染色体、基因异常,仅优质胚胎才能进一步发育至囊胚期^[18]。本研究中由于卵裂期的胚胎数目较少,共17例,因此其妊娠结局统计偏倚较大。本研究胚胎质量的评估主要依靠形态学观察,如细胞碎片比例、细胞数目及均匀度等,但仅靠形

表5 FET患者临床妊娠成功的多因素Logistic回归分析

Table 5 Multivariate logistic regression analysis of successful clinical pregnancy in FET patients

Variable	Odds ratio	95%CI	P
Quality	2.82	(0.93-8.54)	0.067
Junction zone D^*_{mean} .bin	0.20	(0.07-0.59)	0.003

Junction zone D^*_{mean} .bin indicates the categorized form of the continuous Junction zone D^*_{mean} variable, dichotomized using a clinically defined cut-off value of $43.33 \times 10^{-3} \text{ mm}^2/\text{s}$.

态依赖性较高,Zhang等^[17]结合了年龄、BMI、移植胚胎的类型和数量、子宫内膜厚度、以及子宫内膜和子宫下血流的数量等参数,构建了列线图模型来预测FET患者的临床妊娠结局,其训练队列的AUC为0.698,而本研究的AUC值为0.73,且IVIM-DWI可以分离水分子的真实扩散与微循环的灌注效应,为无创评估组织微观结构及血流动力学提供

态评分有一定局限性,如无法评估后续发育过程中的染色体异常^[19]。本研究中优质胚胎45枚,32枚(71%)获得较好的早期妊娠结局,非优质胚胎25枚中10枚(40%)早期妊娠成功,进一步说明仅用胚胎形态学评分不足以说明妊娠结局。

胚胎移植早期的成功着床除了优质的胚胎质量外,还需要良好的内膜容受及胚胎与内膜间的交互作用^[3]。内膜容受性是指内膜对胚胎的接受能力,使其能够为胚胎发育和胎盘形成提供最佳环境。前期临床通过各种方法寻找内膜容受的标志物,超声无创及简便,是最常用的评估方法,包括HCG注射当日内膜厚度、内膜体积、内膜形态(三线征)、内膜及内膜下血供(搏动指数/阻力指数、血管密度、流动指数)、内膜蠕动波等^[20]。胚胎种植后早

期妊娠时,体内孕激素诱导血管扩张,螺旋动脉分支增多,子宫肌层各段血流丰富,血管增宽,为胚胎提供充足血供。Wang等^[21]研究表明,子宫内膜及内膜下均可检测到血流的患者具有较高的妊娠率及着床率。这与本研究结果类似,子宫内膜及结合带血流灌注均高于未妊娠组。Ke等^[22]用多普勒超声发现在围移植期内膜血流灌注尤其是结合带区的血流是妊娠结局的独立预测因子。且Craciunas等^[20]的Meta分析也证明,子宫内膜的VI、FI和VFI在不同临床妊娠结局组间无明显差异,而子宫结合带的VI值在妊娠组中较低、FI值在妊娠组中较高、VFI值两组类似。子宫结合带由基底层内膜和内1/3肌层构成,主要为子宫基底动脉供血,进一步形成螺旋状动脉到达子宫内膜表面,子宫结合带血供最为丰富且决定了内膜螺旋状动脉的血供。因此本研究中子宫结合带的血流灌注参数较子宫肌层及内膜具有相对较高的预测效能。

超声评估血流主要依据可以测量的大血管,而对于血管周围组织间隙内微循环的灌注情况无法评估,但微循环的血流灌注情况往往更能反映着床过程中胚胎与内膜间的交互联系。IVIM-DWI可以通过检测水分子的扩散方向和尺度,直接反映组织的微循环灌注变化^[23]。前期尚未有文章报道IVIM-DWI微循环灌注参数与胚胎移植临床妊娠成功之间的关系。本研究结果显示子宫结合带 D^* 值具有相对较高的早期妊娠预测效能。Lee等^[24]认为 D^* 值与组织微血管密度高度相关($r=0.782$);而微血管密度在前期研究中被证明与胚胎着床密切相关^[25]。因此推测子宫结合带的 D^*_{mean} 可以较好地反映子宫内膜容受性,与临床妊娠结局密切相关。 f 值可以反映血管的密度及微血管生成的速率^[15],既往研究表明, f 值的降低可以反映组织毛细血管网络的损伤及血流阻力的增加^[26]。本研究结合带 f 值直方图分析并没有出现统计学上的显著差异,但未妊娠组较临床妊娠组表现出更低的趋势,相信后续扩大样本量的研究能进一步证实该结果。

本研究根据子宫结合带 D^*_{mean} cut-off值 $43.33 \times 10^{-3} \text{ mm}^2/\text{s}$ 作为截断值将受试者分为高子宫结合带 D^*_{mean} 组及低子宫结合带 D^*_{mean} 组,可以看到低子宫结合带 D^*_{mean} 与次优胚胎组合的早期临床妊娠率明显低于高子宫结合带 D^*_{mean} 与优质胚胎的组合(17% vs. 73%)。而在相同胚胎质量下,高子宫结合带 D^*_{mean} 组临床妊娠率相比低子宫结合带 D^*_{mean} 组有提高,且提升作用在次优胚胎组中更显著,提高了

36%。因此,改善FET患者围移植期子宫内膜及结合带血流灌注可能是改善早期妊娠结局的潜在干预方向。

本研究中胚胎质量联合子宫结合带 D^* 值能显著提高妊娠结局的预测效能预测(AUC=0.73),但是预测效能并不是非常高,原因可能是因为本研究入组的病例数量尚有限;对胚胎着床的影响因素评估不完整,仅纳入了胚胎质量的形态学评估、内膜容受中的血流灌注评估。但是本研究初步显示了IVIM-DWI在FET胚胎移植妊娠结局中的潜在价值。胚胎质量的形态学评估联合MRI评估的内膜容受中的微循环血流灌注信息在预测临床妊娠结局中具有一定价值。随着功能MRI技术的发展以及纳入更多的病例数,相信MRI在FET胚胎移植结局预测中的价值将进一步得到提升和验证。

本研究具有以下局限性:①样本量较小,特别是卵裂期的样本仅17例,冻胚发育周期对于妊娠结局的预测可能不准确,需要纳入更多的样本量来验证本研究结果;②缺乏超声参数,如超声的流速、阻力指数、内膜蠕动等参数,继续收集超声的相关参数,并将在后续研究中进一步探索超声联合MRI特征在妊娠结局预测中的效能;③虽然参照之前研究纳入了较多的临床指标如胚胎质量、胚胎类型、E2、P等,但是仍有部分指标如移植后血HCG值、多胎妊娠、精子活力、自身免疫异常、生殖道感染等未纳入;后续研究将进一步完善临床指标;④现有的观察终点是临床妊娠,后续将进一步以活产率为观察终点进行深入研究。

综上所述,IVIM-DWI参数可无创评估FET患者子宫肌层、结合带及内膜微循环灌注特征,子宫结合带 D^*_{mean} 值联合胚胎质量参数可提升FET妊娠结局的预测效能。IVIM-DWI参数在FET胚胎移植临床妊娠结局中具有潜在的预测价值。

利益冲突声明:

所有作者声明不存在利益冲突。

Conflict of Interests:

All authors declare that there is no conflict of interests.

作者贡献声明:

吴飞云、陈婷、马翔设计研究方案,对稿件重要内容进行审阅;邵文慧收集、整理、分析数据,撰写文章初稿;宋佳成、张爱宁和王菁对稿件进行修改;陆遥收集文章数据;徐义程数据分析、数据可视化。

Author's Contributions:

WU Feiyun, CHEN Ting, and MA Xiang designed the research plan and reviewed the important contents of the manu-

script; SHAO Wenhui collected, sorted, and analyzed the data and wrote the first draft of the article; SONG Jiacheng, ZHANG Aining, and WANG Jing revised the manuscript; LU Yao collected the data for the article; XU Yicheng performed data analysis and data visualization.

[参考文献]

- [1] QIAO J, WANG Y, LI X, et al. A Lancet Commission on 70 years of women's reproductive, maternal, newborn, child, and adolescent health in China[J]. *Lancet*, 2021, 397(10293): 2497-2536
- [2] RIESTENBERG C, KROENER L, QUINN M, et al. Routine endometrial receptivity array in first embryo transfer cycles does not improve live birth rate[J]. *Fertil Steril*, 2021, 115(4): 1001-1006
- [3] LU Y, MAO X, HE Y, et al. Efficacy of endometrial receptivity testing for recurrent implantation failure in patients with euploid embryo transfers: study protocol for a randomized controlled trial[J]. *Trials*, 2024, 25(1): 348
- [4] BUI B N, KUKUSHKINA V, MELTSOV A, et al. The endometrial transcriptome of infertile women with and without implantation failure[J]. *Acta Obstet Gynecol Scand*, 2024, 103(7): 1348-1365
- [5] HAAS J, CASPER R F. Observations on clinical assessment of endometrial receptivity [J]. *Fertil Steril*, 2022, 118(5): 828-831
- [6] 钟晓盈, 贾雪敏, 刘海元. 子宫内膜容受性的研究进展[J]. *生殖医学杂志*, 2024, 33(9): 1250-1257
- ZHONG X Y, JIA X M, LIU H Y. Research progress of endometrial receptivity[J]. *Journal of Reproductive Medicine*, 2024, 33(9): 1250-1257
- [7] SILVA MARTINS R, HELIO OLIANI A, VAZ OLIANI D, et al. Subendometrial resistance and pulsatility index assessment of endometrial receptivity in assisted reproductive technology cycles[J]. *Reprod Biol Endocrinol*, 2019, 17(1): 62
- [8] WANG J, XIA F, ZHOU Y, et al. Association between endometrial/subendometrial vasculature and embryo transfer outcome: a meta-analysis and subgroup analysis[J]. *J Ultrasound Med*, 2018, 37(1): 149-163
- [9] WU J, SHENG J, WU X, et al. Ultrasound assessed endometrial receptivity measures for the prediction of in vitro fertilization embryo transfer clinical pregnancy outcomes: a metaanalysis and systematic review[J]. *Exp Ther Med*, 2023, 26(3): 453
- [10] 张亚兰, 李秀春, 刘昌荣. 超声造影检测子宫内膜及内膜下血流灌注评价子宫内膜容受性的应用研究[J]. *中国医学装备*, 2017, 14(1): 7-11
- ZHANG Y L, LI X C, LIU C R. An application study on assessment for endometrialreceptivity by detecting endometrial and sub-endometrial perfusionwith contrast-enhanced ultrasound [J]. *China Medical Equipment*, 2017, 14(1): 7-11
- [11] DOLCIAMI M, CAPUANI S, CELLI V, et al. Intravoxel incoherent motion (IVIM) MR quantification in locally advanced cervical cancer (LACC): preliminary study on assessment of tumor aggressiveness and response to neoadjuvant chemotherapy[J]. *J Pers Med*, 2022, 12(4): 638
- [12] ZIMMERMANN J, REOLON B, MICHELS L, et al. Intravoxel incoherent motion imaging in stroke infarct core and penumbra is related to long-term clinicaloutcome[J]. *Sci Rep*, 2024, 14(1): 29631
- [13] DENG J, ZHANG A, ZHAO M, et al. Placental perfusion using intravoxel incoherent motion MRI combined with Doppler findings in differentiating between very low birth weight infants and small for gestational age infants [J]. *Placenta*, 2023, 135: 16-24
- [14] 张瑾, 张璇, 陆超, 等. 体素内不相干运动成像诊断胎盘植入及不同植入区域的应用价值[J]. *南京医科大学学报(自然科学版)*, 2023, 43(9): 1285-1290
- ZHANG J, ZHANG X, LU C, et al. Application value of intravoxel incoherent motion imaging in diagnosing placental implantation and different implantation regions[J]. *Journal of Nanjing Medical University (Natural Sciences)*, 2023, 43(9): 1285-1290
- [15] LI X, LI L, HUANG L, et al. Field-of-view optimized and constrained undistorted single shot intravoxel incoherent motion diffusion-weighted imaging of the cervix during the menstrual cycle: a prospective study[J]. *Magn Reson Imaging*, 2024, 107: 47-54
- [16] 徐何荣, 端木家苗, 李宏慧, 等. 新鲜周期D3卵裂期胚胎细胞数对D5囊胚质量和临床结局的影响[J]. *生殖医学杂志*, 2025, 34(2): 143-149
- XU H R, DUANMU J M, LI H H, et al. The impact of cell number of D3 cleavage-stage embryo on D5 blastocyst quality and clinical outcomes in fresh cycle[J]. *Journal of Reproductive Medicine*, 2025, 34(2): 143-149
- [17] ZHANG Q, WANG X, ZHANG Y, et al. Nomogram prediction for the prediction of clinical pregnancy in freeze-thawed embryo transfer [J]. *BMC Pregnancy Childbirth*, 2022, 22(1): 629
- [18] XIE Q, JIANG W, JI H, et al. Perinatal outcomes of singletons born after blastocyst or cleavage-stage embryo transfer in FET cycles [J]. *Eur J Obstet Gynecol Reprod Biol*, 2022, 271: 265-270
- [19] 温美婷, 孙虹. 辅助生殖中胚胎质量评估方法的研究

- 进展[J].中国计划生育和妇产科,2023,15(1):47-51
- WEN M T, SUN H. Research progress on embryo quality assessment methods in assisted reproduction[J]. Chinese Journal of Family Planning & Gynecotokology, 2023, 15(1): 47-51
- [20] CRACIUNAS L, GALLOS I, CHU J, et al. Conventional and modern markers of endometrial receptivity: a systematic review and meta-analysis[J]. Hum Reprod Update, 2019, 25(2): 202-223
- [21] WANG L, QIAO J, LI R, et al. Role of endometrial blood flow assessment with color Doppler energy in predicting pregnancy outcome of IVF-ET cycles[J]. Reprod Biol Endocrinol, 2010, 8: 122
- [22] KE X, LIANG X F, LIN Y H, et al. Pregnancy prediction via ultrasound-detected endometrial blood for hormone replacement therapy-frozen embryo transfer: a prospective observational study[J]. Reprod Biol Endocrinol, 2023, 21(1): 112
- [23] BAO Y, PANG Y, SUN Z, et al. Functional diagnosis of placenta accreta by intravoxel incoherent motion model diffusion-weighted imaging[J]. Eur Radiol, 2021, 31(2): 740-748
- [24] LEE H J, RHA S Y, CHUNG Y E, et al. Tumor perfusion-related parameter of diffusion-weighted magnetic resonance imaging: correlation with histological microvessel density[J]. Magn Reson Med, 2014, 71(4): 1554-1558
- [25] DEANS R, MOSES D, SACH T A, et al. Perfusion magnetic resonance imaging in Asherman syndrome[J]. Aust N Z J Obstet Gynaecol, 2024, 64(4): 341-346
- [26] HU Q, JIANG P, FENG Y, et al. Noninvasive assessment of endometrial fibrosis in patients with intravoxel incoherent motion MR imaging[J]. Sci Rep, 2021, 11(1): 12887

[收稿日期] 2025-05-03

(本文编辑:唐震)

(上接第1394页)

- [28] MUSGROVE E A, ELIZABETH C C, BARRACLOUGH J, et al. Cyclin D as a therapeutic target in cancer[J]. Nat Rev Cancer, 2011, 11(8): 558-572
- [29] FERGUSON K M, GILLEN S L, CHAYTOR L, et al. Palbociclib releases the latent differentiation capacity of neuroblastoma cells[J]. Dev Cell, 2023, 58(19): 1967-1982
- [30] DAS S, NEELAMEGAM K, PETERS W N, et al. Depletion of cyclic-GMP levels and inhibition of cGMP-dependent protein kinase activate p21^{Cip1}/p27^{Kip1} pathways and lead to renal fibrosis and dysfunction[J]. FASEB J, 2020, 34(9): 11925-11943
- [31] DESHMUKH D, XU J, YANG X, et al. Regulation of p27 (Kip1) by ubiquitin E3 ligase RNF6[J]. Pharmaceutics, 2022, 14(4): 802
- [32] MIAO H H, LIU W B, JIAO X H, et al. Neonatal exposure to propofol interferes with the proliferation and differentiation of hippocampal neural stem cells and the neurocognitive function of rats in adulthood *via* the Akt/p27 signaling pathway[J]. Biomed Environ Sci, 2022, 35(4): 283-295
- [33] EL-WAKIL A, FRANCIUS C, WOLFF A, et al. The GATA2 transcription factor negatively regulates the proliferation of neuronal progenitors[J]. Development, 2006, 133(11): 2155-2165
- [34] EZOE S, MATSUMURA I, NAKATA S, et al. GATA-2/estrogen receptor chimera regulates cytokine-dependent growth of hematopoietic cells through accumulation of p21 (WAF1) and p27 (Kip1) proteins[J]. Blood, 2002, 100(10): 3512-3520

[收稿日期] 2024-11-30

(本文编辑:陈汐敏)